BNL-43153
OG-1081

S.U. Chung

Double prompt photon production at high transverse momentum by π^- on protons at 280 GeV/c

WA70-collaboration

E.Bonvin[5], R.Bopp[1], L.J.Carroll[3], A.J.Cass[3], S.U.Chung[1], M.Donnar[1]; P.A.Dorsaz[1], M.E.Feliks[2], L.Fluri[5], J.N.Jackson[3], M.N.Kienzle-Focacci[1], J.G.Lynch[2], M.Martin[1], L.Mathys[1], P.J.Negus[2], L.Perini[4], R.Poultney[3], W.H.Range[3], L.Rosselet[1], S.W.Snow[3], A.S.Thompson[2], R.M.Turnbull[2] and M.Werlen[1]

Geneva, 1 June 1988

Abstract: A search for pairs of high p_T prompt photons produced in hydrogen by a 280 GeV/c incident π^- beam has been carried out using a fine-grained electromagnetic calorimeter and the Omega spectrometer at the CERN SPS. Clear evidence for the existence of such events is found with a six standard deviation signal for $p_T > 3.0$ GeV/c. The cross-sections are consistent with beyond leading order QCD calculations. A discussion on the determination of α_s is also presented.

Submitted to the XXIV International Conference on High Energy Physics, 4–10 August, 1988, Münich, Germany.

[1] University of Geneva, D.P.N.C., CH-1211 GENEVE, Switzerland
[2] University of Glasgow, Dept. of Physics and Astronomy, GLASGOW, G12 8QQ, UK
[3] University of Liverpool, Dept. of Physics, LIVERPOOL, L69 3BX, UK
[4] CERN,CH – 1211 GENEVE 23, Switzerland
[5] University of Neuchâtel, CH-2000 NEUCHATEL, Switzerland

1. Introduction

Double prompt photon production by the QED annihilation subprocess $q\bar{q}\rightarrow\gamma\gamma$ (fig.1a) was discussed as early as 1971 in the framework of the parton model [1]. Measurement of the rate of double photon production in hadron-hadron collisions was first proposed as a means of determining the quark charges but its importance for other aspects of QCD has been emphasized by many authors [2]. In particular there is the possibility of determining the strong coupling constant α_s by comparing this subprocess with $q\bar{q}\rightarrow\gamma g$ (fig.1b). However the measurements are difficult due to the small production cross-section relative to $\gamma\gamma$ background from the abundant $\pi^0\pi^0$ production. In QCD theory it has been shown that the subprocess $gg\rightarrow\gamma\gamma$ [3] (box diagram fig.1c) as well as photon bremsstrahlung from a quark [4] may also contribute to double photon production. Beyond leading logarithm (BLL) calculations [5,6] allow a quantitative comparison of the data with QCD theory.

Photon pairs have been observed in pp collisions at the CERN ISR [7] with a two standard deviation signal. More recently the CERN NA3 experiment [8] has reported a three standard deviation signal for $p_T > 1.8$ GeV/c in both π^- and p beams with an incident momentum of 200 GeV/c on a carbon target. The cross-section measured by NA3 was higher than predicted by BLL QCD calculations.

The present experiment, using a 280 GeV/c hadron beam, a fine-grained electromagnetic calorimeter and the Omega spectrometer, has accumulated a sample of $\pi^-p\rightarrow\gamma\gamma X$ events with a sensitivity of 7.7 $pbarn^{-1}$. The range of centre of mass rapidity of each photon is $-1.0 < y^* < 1.25$ and the transverse momentum is $p_{T1} > 3.0$ GeV/c and $p_{T2} > 2.75$ GeV/c for the photon with higher and lower p_T respectively.

2. Experimental system

The experimental layout, shown in fig.2, has been described in detail elsewhere [9] . It consists of a fine-grained electromagnetic calorimeter providing a large p_t and y^* acceptance, a shower separation

down to 2 cm and efficient photon detection for energies greater than 500 MeV. The calorimeter is composed of four quadrants (Q1 − Q4) segmented in depth into three parts to distinguish between hadronic and electromagnetic showers. A 16 m^2 MWPC detects charged particles entering the calorimeter. The Omega spectrometer provides charged track reconstruction and the determination of the interaction vertex thus allowing an accurate definition of the transverse momentum of electromagnetic showers.

For triggering purposes [10] each quadrant is divided into 16 cells by grouping the photomultiplier signals, and a selection can be made in each cell for transverse energy E_T above a given threshold. Photon pairs have been selected by a trigger requiring $E_T > 1.7$ GeV in both quadrants 1 and 3 and $E_T > 2.0$ GeV for quadrants 2 and 4. The higher threshold was used in quadrants 2 and 4 in order to reduce spurious triggers from low momentum charged particles swept into the calorimeter by the magnetic field. In order to resolve the spatial ambiguities of the orthogonal readout of the calorimeter for multishower events, a time-of-flight (TOF) system [11] measures the transit time of the light along the scintillator elements of the first segment.

3. Data selection

The π^-p data used for the present analysis correspond to a sensitivity of 7.7 $pbarn^{-1}$.

The event reconstruction and data selection followed the same procedure as that used for the analysis of high p_T π^0 [12] and prompt photon events [13]. A sample of double photon events has been obtained by requiring that :

a. the time-of-flight information is consistent with a single beam interaction in the hydrogen target;

b. an interaction vertex can be found inside the target using the reconstructed charged tracks;

c. there are at least two trigger "photon showers" with $p_t > 1.8$ GeV/c in two opposite quadrants(Q1 − Q3) or (Q2 − Q4). Where a shower has been defined to be a "photon shower" when less than 20% of the energy deposited in the calorimeter appears in the third segment and there is no corresponding hit in the 16 m^2 MWPC within a 3 cm radius. The shower with maximum p_T inside a trigger cell was defined as the "trigger shower".

3.1 Prompt photon reconstruction

A trigger shower was considered as a prompt photon candidate if all the following requirements were satisfied :

a. the trigger shower has $p_T > 2.75$ GeV/c, this cut has been established by background estimates;

b. the effective mass with any photon giving a decay energy asymmetry $|E_{\gamma 1} - E_{\gamma 2}| / (E_{\gamma 1} + E_{\gamma 2}) < 0.95$ was outside the π^0 mass range (135 ± 50) MeV;

c. the effective mass with any photon having $E > 2.0$ GeV and giving an asymmetry < 0.8 was outside the η mass range (550 ± 100) MeV;

d. the shower width corresponded to a single electromagnetic shower (σ < 2 cm);

e. the shower position was inside a fiducial region extending to 5 cm from the edges of each quadrant.

3.2 π^0 reconstruction

The $\gamma\gamma$ signal is contaminated by high p_T hadrons decaying electromagnetically and not fully reconstructed. This background was estimated by a detailed Monte-Carlo, with the normalization being obtained from a π^0 data sample.

In order to define such a π^0 sample with a low background, the trigger shower was combined with all photon showers in the same quadrant provided that the shower pair had a $p_T > 2.75$ GeV/c, an asymmetry < 0.9 and an effective mass in the range (135 ± 50) MeV (fig.3a). Because the initial selection of events required the trigger photon of the π^0 to have $p_T > 1.8$ GeV/c, the decay asymmetry distribution is not flat (fig.3b).

3.3 High p_T pairs

The high p_T π^0s and γs obtained by such definitions provide four classes of reconstructed events :

$$\pi^0\pi^0 \ , \ \pi^0\gamma \ , \ \gamma\pi^0 \ , \ \gamma\gamma$$

where the two particles are ordered in p_t with $p_{T1} > p_{T2}$. The number of reconstructed events after correction for background under the π^0 peak (~5% for π^0_1, ~12% for π^0_2) is given in table 1 for $p_{T1} > 3.0$ GeV/c and $p_{T2} > 2.75$ GeV/c. The higher cut for p_{T1} avoids resolution effects in the lower p_T bin.

Table 1: *Data for $p_{T1} > 3.0$ GeV/c and $p_{T2} > 2.75$ GeV/c*

Class of events	Number of events
$\pi^0\pi^0$	1997
$\pi^0\gamma$	614
$\gamma\pi^0$	547
$\gamma\gamma$	282

The p_T distribution of the particles for each class of event is presented in fig.4; both p_{T1} and p_{T2} have been included.

4. Double prompt photon acceptances

In order to evaluate the acceptance, detection and recontruction efficiencies of the $\gamma\gamma$ events, the leading order annihilation $q\bar{q}\rightarrow\gamma\gamma$ and the box $gg\rightarrow\gamma\gamma$ diagrams were generated using the TWISTER version of the LUND Monte-Carlo [14,15]. The y^* distribution, as generated by the Monte-Carlo and as reconstructed after the simulation of all experimental effects, is shown in fig.5a for both photons in the full p_T interval. The y^* acceptance extends from -1.0 to 1.25. In the analysis the data are corrected by the experimental acceptance and then normalized to the whole range of y^* allowed by kinematics. The full efficiency is shown in fig.5b as a function of p_T. The percentages of $\gamma\gamma$ losses relative to the total number of generated events are summarized in table 2 .

Table 2: $\gamma\gamma$ *losses for* $p_{T1} > 3.0$ *GeV/c and* $p_{T2} > 2.75$ *GeV/c*

γ conversion	13%
γ outside calorimeter	27%
$\gamma\gamma$ not in opposite-side quadrants	5%
Fiducial cuts	17%
Accidental triggers rejection	3%
Misidentification of γ	1%

5. Two photon background

Background in the double prompt photon signal arises from the decay of high p_t hadrons, mainly $\pi^0\rightarrow\gamma\gamma$, $\eta\rightarrow\gamma\gamma$, $\eta'\rightarrow\gamma\gamma$, $\omega\rightarrow\pi^0\gamma$, which are abundantly produced in π^-p hard scattering. Leading particles of the fragmentation following a hard parton-parton scattering will mainly contribute to the $\pi^0\pi^0$ sample, but they will also appear as $\pi^0\gamma$, $\gamma\pi^0$ or $\gamma\gamma$ events when one or two decay photons escape detection.

Another source of background is prompt photon production where a high p_T prompt photon is associated with a photon from the decay of a high p_T hadron. This is the main contribution to the background at high p_T.

Two kinds of Monte-Carlo events were generated using QCD leading order diagrams with the LUND fragmentation model [14] . The first, referred to as "MC1", simulates all parton-parton leading order diagrams with fragmentation into a π^0, η or any other hadron decaying to a high p_T γ. The second, referred to as "MC2", generates single prompt photon events. All particles have been traced to the calorimeter through a full detector simulation including materialization of γs, secondary interactions and trigger effects. The longitudinal and transverse development of electromagnetic and hadronic showers have been parametrized using experimental data and the Monte-Carlo events were processed with the same chain of programs as real data.

The normalization factors A and B of both Monte-Carlos are obtained by minimizing the following chi-square:

$$\chi^2 = \sum_{i=1}^{6} \sum_{j=1}^{3} \frac{(\text{data} - A.MC1 - B.MC2)_{ij}^2}{\sigma_{ij}^2}$$

with the index i running over all p_t bins, index j running over the three samples $\pi^0\pi^0$, $\gamma\pi^0$, $\pi^0\gamma$ (fig.4a-c). The errors σ_{ij} take into account the data and the Monte-Carlo statistics. The Monte-Carlo generations reproduce the experimental p_T distributions for $p_T > 3.0$ GeV/c with a global chi-square of 11.6 / 16 d.o.f (table 3 and fig.4a-c). The ratio (B/A) of the Monte-Carlo normalization factors found, corrected by the relative generated statistics, gives (6.9±0.9)%. This value is a measure of the (γ/π^0) production ratio integrated for the range above $p_T = 3.0$ GeV/c. It can be compared to the single particle (γ/π^0) ratio obtained by this experiment for $p_T > 4.0$ GeV/c [13]; extrapolating the single γ and π^0 cross-sections as functions of p_T to 3.0 GeV/c, the integrated γ/π^0 ratio is (5±2)%.

The background in the $\gamma\gamma$ sample is then assumed to be entirely described by the two Monte-Carlos. The major part of the background is (~75%) due to pattern recognition ambiguities in shower reconstruction. The relative contributions of the different final states to the $\gamma\gamma$ background are given in table 4.

Table 3: *Relative contribution of the two Monte-Carlo generations*

Class	MC1(%)	MC2(%)	partial χ^2
$\pi^0\pi^0$	99.8	0.2	5.0
$\pi^0\gamma$	85.0	15.0	2.8
$\gamma\pi^0$	60.0	40.0	3.8

Table 4: *Percentage of $\gamma\gamma$ background versus generated particles*

Particles	Background(%)	Particles	Background(%)
$\gamma\pi^0$	30	$\pi^0\pi^0$	23
$\eta\pi^0$	18	$\eta\eta$	7
$\gamma\eta$	8	$\omega\pi^0$	5
$\eta'\pi^0$	4	other hadrons	5

The p_T distributions of the backgrounds are also drawn in fig.4d. Both background contributions are shown separately in fig.4d, their weighted sum (dashed dotted line) being well below the experimental data.

6. Results

6.1 Statistical significance

The integrated statistics with $p_{T1} > 3.0$ GeV/c and $p_{T2} > 2.75$ GeV/c is presented in table 5 together with the Monte-Carlo backgrounds. The $\gamma\gamma$ signal is statistically significant (6 standard deviations) after a background subtraction of about 50%. These results include the statistical errors on the data and on the Monte-Carlo. The corresponding cross-section $\Delta\sigma$, given in table 5, is computed for the full kinematically allowed y^* range.

Table 5: $\gamma\gamma$ *signal for* $p_{T1} > 3.0$ *GeV/c and* $p_{T2} > 2.75$ *GeV/c*

$\gamma\gamma$ candidates	282±17
background :	
from MC1	84±13
from MC2	60±8
$\gamma\gamma$ signal	138±23
$\Delta\sigma(\pi^- p \to \gamma\gamma X)$	54±8.8 pb

The uncertainty in the background subtraction is included in the quoted error. The systematic error on the integrated cross-section is estimated to be ± 15%, taking into account the various normalization effects added in quadrature; a detailed description of systematic errors is given in reference 12 .

Additional contributions to the mass spectrum of the $\gamma\gamma$ continuum coming from heavy resonances decaying into $\gamma\gamma$ are not observed in the data (fig.6).

6.2 Cross-sections and comparison with QCD calculations

The data have been compared to BLL QCD calculations [6] which include the Born term (fig.1a) with its $O(\alpha_s)$ corrections as well as the $O(\alpha_s^2)$ box diagram (fig.1c) using the Duke-Owens set I structure functions [18] with $\Lambda = 200$ MeV and $Q^2 = p_T^2$. The sensitivity of the predictions to the Q^2 scale is expected to be small for the $\gamma\gamma$ production. In this calculation the bremsstrahlung contributes about 5% to the total cross-section; the box diagram contributes 12% at $p_{T1} = 3.0$ GeV/c, rapidly decreasing to less than 1% at $p_{T1} = 7.0$ GeV/c.

The cross-section calculations of reference 6 have been integrated over the variable:

$$\Delta\phi = \phi_1 - \phi_2$$

where ϕ_1, ϕ_2 are the azimuthal angles of the two photons. In order to compare the data with this calculation integrated over the same kinematical region, a cutoff on the variable z defined as:

$$z = -\vec{p}_{T1}\cdot\vec{p}_{T2}/p_{T1}^2 = -(p_{T2}/p_{T1}).\cos\Delta\phi$$

has been applied to the data at $z_{min} = 2.75/p_{T1}$ since the selection requires $p_{T2} > 2.75$ GeV/c. The requirement $z > z_{min}$ rejects ~20% of the events.

The differential cross-section $d\sigma/dp_T$ as a function of p_T, for the full y^* and ϕ ranges ($z > z_{min}$) is presented in fig.7 and in table 6. Both γs are counted in the cross-section. This cross-section integrated from $p_T > 3.0$ GeV/c yields :

$$(69 \pm 11.5) \text{ pb}$$

to be compared with a predicted value of 57.8 pb for BLL QCD calculations while the leading logarithm $q\bar{q} \to \gamma\gamma$ gives 39.4 pb. The data agree with BLL QCD predictions in absolute value and p_T dependence to within the statistical errors.

Table 6: $\gamma\gamma$ differential cross-section $d\sigma/dp_T$

p_T range GeV/c	$d\sigma/dp_T$ pb/(GeV/c)
3.0 − 3.5	70.0± 17.2
3.5 − 4.0	25.0± 8.6
4.0 − 4.5	17.0± 5.2
4.5 − 5.0	10.0± 3.4
5.0 − 6.0	4.7± 1.4
6.0 − 7.0	1.0± 0.6

6.3 Discussion of α_s

Comparing the leading order diagrams $q\bar{q} \to \gamma g$ and $q\bar{q} \to \gamma\gamma$ (fig.1a,b) one can write [4] :

$$\frac{d\hat{\sigma}/d\hat{t}(q\bar{q} \to \gamma g)}{d\hat{\sigma}/d\hat{t}(q\bar{q} \to \gamma\gamma)} = (4/3)\,(\alpha_s/(\alpha\, e_q^{\,2}))$$

where e_q is the quark charge. These annihilation cross-sections can be obtained from the difference between $\pi^- p$ and $\pi^+ p$ cross-sections. Estimates, based on beyond leading logarithm QCD, show that this difference isolates the annihilation contribution with an accuracy better than 1%. Using the experimental ratio:

$$R = \frac{\sigma(\pi^- p \to \gamma X) - \sigma(\pi^+ p \to \gamma X)}{\sigma(\pi^- p \to \gamma\gamma) - \sigma(\pi^+ p \to \gamma\gamma)}$$

α_s at leading order approximation can be defined as:

$$\alpha_s(LO) = (1/3)\alpha\ R$$

where we have neglected the $d\bar{d}$ annihilation contibutions by taking $e_q = 2/3$. The latter approximation is better than 9% for the numerator of R and 2% for the denominator.

The numerator of R has been obtained from the measured cross-sections of reference 13 . To obtain the denominator, the value of the $\pi^+ p \to \gamma\gamma X$ cross-section is estimated by BLL QCD to be about 10% of the measured $\pi^- p \to \gamma\gamma X$ cross-section [6]. The absence of experimental data on $\sigma(\pi^+ p \to \gamma\gamma X)$ gives a contribution of $\pm 5\%$ to the uncertainty in the denominator. The resulting cross-sections $d\sigma/dp_T$ are given in table 7, without requiring $z > z_{min}$, for $p_T > 4.0$ GeV/c where both channels have been measured. The values of R and $\alpha_s(LO)$ are also given. These values of $\alpha_s(LO)$ have to be interpreted with caution since higher order corrections may give important corrections.

Beyond leading order the cross-sections may be expressed [17] as corrections to the Born term σ_0 and the experimental ratio R is then interpreted as:

$$R = \frac{K_1\sigma_0^{\gamma}}{K_2\sigma_0^{\gamma\gamma}} = \frac{\int F_q(M_1^2)F_{\bar{q}}(M_1^2)\, d\sigma_0^{\gamma}(Q_1^2)\,[1+\alpha_s C^{\gamma}]}{\int F_q(M_2^2)F_{\bar{q}}(M_2^2)\, d\sigma_0^{\gamma\gamma}\,[1+\alpha_s C^{\gamma\gamma}]}$$

where M_1^2 and M_2^2 are the factorization scales of the structure functions F and Q_1^2 is the renormalization scale. Using $M_1^2 = M_2^2 = Q_1^2 = p_T^2$ ($\Lambda = 200$ MeV, $N_f = 4$), as in the previous calculation, the higher order corrections factors are large. The K-factors, defined as $\sigma(\text{BLL} + \text{Born})/\sigma(\text{Born})$, are $K_1 \simeq 1.6$ and $K_2 \simeq 1.5$. However, the Born term multiplied by the K_1-factor does not reproduce the single prompt photon data and the measured $\alpha_s(LO)$, even after correcting by the corresponding K-factors, does not agree with α_s evaluated at $Q^2 = p_T^2$.

The principle of minimal sensitivity [16] was applied to the $q\bar{q} \to \gamma g$ channel to get stable predictions for the cross-sections [17]. This leads to a definition of "optimized" scales for this process

(with $\Lambda = 200$ MeV and Duke-Owens set I structure functions) where the higher order corrections are smaller: $K_1 \simeq 0.9$. The same scales reduce K_2 to $\simeq 1.2$. This choice of scales corresponds to an effective α_s(opt) which minimizes contributions from higher order terms, and is specific to the process considered. The optimization procedure applied to $\sigma(\pi^- p \to \gamma X) - \sigma(\pi^- p \to \gamma X)$ in the kinematical range of this experiment (using $\Lambda = 200$ MeV, $N_f = 4$), gives a renormalization scale:

$$Q^2_1(\text{renormalization}) = 0.49\, p_T^2 - 3.93\, p_T + 8.28$$

where we have fitted the p_T dependence to a second order polynomial. The experimental α_s(LO) should correspond to within a 30% calculation uncertainty (table 7) to the the value of α_s(opt) if the "optimized" scales are justified. Although the measurement errors and the QCD estimates uncertainties do not allow to draw a strong conclusion, the experimental value of α_s(LO) is in fact in better agreement with α_s(opt) than with α_s evaluated at $Q^2 = p_T^2$ ($\Lambda = 200$ MeV, $N_f = 4$).

Table 7: α_s(LO) and comparison with QCD

p_T range Gev/c	$d\sigma/dp_T$ pb $q\bar{q} \to \gamma g$	$d\sigma/dp_T$ pb $q\bar{q} \to \gamma\gamma$	R expt.	α_s(LO) expt.	$\alpha_s(Q^2 = p_t^2)$	α_s(opt)
4.0 − 4.5	1930 ± 196	10.7 ± 2.5	180 ± 46	0.44 ± 0.11	0.193	0.46 ± 0.14
4.5 − 5.0	872 ± 106	5.5 ± 1.6	159 ± 50	0.39 ± 0.12	0.187	0.39 ± 0.11
5.0 − 6.0	251 ± 42	2.5 ± 0.7	102 ± 32	0.25 ± 0.08	0.180	0.31 ± 0.09

7. Conclusion

The WA70 experiment has observed a six standard deviation signal for the production of double prompt photons having $p_{T1} > 3.0$ GeV/c and $p_{T2} > 2.75$ GeV/c in $\pi^- p$ collisions. The measured cross-sections agree with beyond leading order QCD predictions (using $\Lambda = 200$ MeV and Duke-Owens set I structure functions) both in magnitude and in p_T dependence. The comparison of the $\pi^- p \to \gamma\gamma X$

cross-section with that for $\pi^- p \to \gamma X$ production allows a determination of an effective QCD strong coupling constant α_s. The values obtained are consistent with the QCD perturbative theory using optimized scales.

Acknowledgements

It is a pleasure to thank P.Aurenche and M.Fontannaz for helpful and stimulating discussions.

We are grateful to the members of the Omega support group as well as the EA support group for their assistance throughout the experiment.

We gratefully acknowledge the provision of computing facilities by CERN, RAL and University of Geneva as well as financial support from CERN, the United Kingdom SERC and the Swiss National Science Foundation.

This research supported in part by the U.S. Dept. of Energy under Contract No. DE-AC02-76CH00016.

References

[1] S.M.Berman,J.D.Bjorken and J.B.Kogut:Phys.Rev.D4,3388(1971)

[2] K.S.Soh,P.Y.Pac,H.W.Lee and J.B.Choi:Phys.Rev.D18,751(1978)
M.Krawczyk and W.Ochs : Phys.Lett.B, 79, 119(1978)
S.Hemmi: Prog. theor. Phys. 23, 1073(1980).
C.Carimalo,M.Crozon,P.Kessler and J.Parisi:Phys.Lett.B 98, 105(1981)

[3] B.L.Combridge:Nucl.Phys.B 174, 243(1980)

[4] E.L.Berger,E.Braaten and R.D.Field:Nucl.Phys.B239,52(1984)3

[5] A.P.Contogouris,L.Marleau and B.Pire : Phys.Rev.D 25, 2459(1982).

[6] P.Aurenche, R.Baier, A.Douiri,M.Fontannaz, D.Schiff: Z.Phys.C 29, 459 (1985). We thank the authors for allowing us to use their computer program.

[7] C.Kourkoumelis et al : Z.Phys.C 16, 101(1982).
T.Akesson et al : Z.Phys.C 32, 491(1986).

[8] J.Badier at al.: Phys.Lett.164B, 184 (1985)

[9] M.Bonesini et al., Nucl.Instr. and Meth.A 261, 471(1987).

[10] P.Béné et al.: "High p_T trigger electronics for a large orthogonal readout electromagnetic calorimeter", CERN−EP/87−200,to be published in Nucl. Instrum. Methods.

[11] M.Bonesini et al., Nucl.Instr. and Meth.A 263, 325(1988).

[12] M.Bonesini et al., Z.Phys.C. 37, 39(1987).

[13] M.Bonesini et al.,Z.Phys.C 37, 535 (1988).

[14] H.U.Bengtsson, G.Ingelman, T.Sjöstrand: The Lund Monte-Carlo for high-p_T scattering, PYTHIA version 4.1, update of H.U.Bengtsson and G.Ingelman: Comp. Phys. Comm. 34, 251 (1985); T.Sjöstrand: Jet fragmentation, JETSET version 6.2, update of T.Sjöstrand: Comp. Phys. Comm. 27, 243 (1982)

[15] G.Ingelman:"TWISTER a Monte-Carlo for QCD high p_T scattering", DESY 86−131.

[16] P.M.Stevenson:Phys.Rev.D23,2916(1981)
H.D.Politzer:Nucl.Phys.B194,493(1982)
P.Stevenson and H.D.Politzer:Nucl.Phys.B277,758(1986)

[17] P.Aurenche,R.Baier,M.Fontannaz,D.Schiff:Nucl.Phys.B286,509(1987)

[18] D.W.Duke and J.F.Owens, Phys. Rev. D30, 49 (1984) J.F.Owens, Phys. Rev. D30, 943 (1984)

Figure captions

1. QCD diagrams

a)The leading order (Born) annihilation diagram for $q\bar{q} \to \gamma\gamma$

b)The leading order (Born) annihilation diagram for $q\bar{q} \to \gamma g$

c)The box diagram for $gg \to \gamma\gamma$.

2. a) The experimental layout.

b) The electromagnetic calorimeter.

3. a) The effective mass spectrum of the higher p_T triggering photon with all photons of the same quadrant.

b) The π^0 decay asymmetry $|E_{\gamma 1} - E_{\gamma 2}| / (E_{\gamma 1} + E_{\gamma 2})$ for the π^0 with higher p_T (π^0_1). Superimposed to the data (full line) are the Monte-Carlo events with their statistical errors.

4.Transverse momentum p_T distributions of π^0s and γs for the four classes of events:

a) $\pi^0\pi^0$ b) $\pi^0\gamma$ c) $\gamma\pi^0$ d) $\gamma\gamma$. Both particles are plotted in the histograms.The data are drawn as as black points with their statistical errors. The Monte-Carlo "MC1" is presented with crosses on which a full line is drawn to guide the eye. The Monte-Carlo "MC2" is presented as squares and connected by a dashed line. The sum of the two Monte-Carlos is indicated as a dashed dotted line.

5. Acceptance of $\gamma\gamma$ events as given by the Lund Monte-Carlo:

a) generated (full line) and reconstructed (dashed line) events as function of y^* integrated for $p_T > 2.75$ GeV/c.

b) ratio of reconstructed over generated events as a function of p_T for the full y^* range.

6. $\gamma\gamma$ invariant mass spectrum for $p_T > 2.75$ GeV/c without background subtraction, compared to the Monte-Carlo (MC1,MC2 and $MC_{\gamma\gamma}$ properly normalized).

7. The $\gamma\gamma$ cross-section $d\sigma/dp_T$, where p_T is the transverse momentum of either of the two prompt photons. The dashed line is the prediction of the $q\bar{q} \to \gamma\gamma$ Born term; the full line is the prediction of beyond leading logarithm calculations of reference 6 .

a) $q\bar{q} \rightarrow \gamma\gamma$

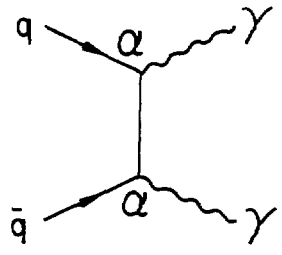

b) $q\bar{q} \rightarrow \gamma g$

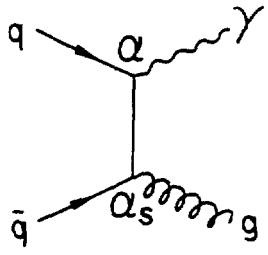

c) $gg \rightarrow \gamma\gamma$

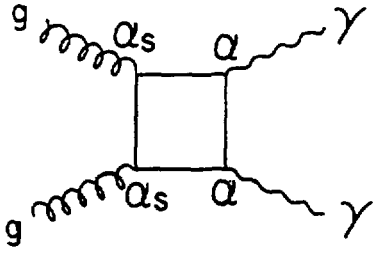

FIG. 1

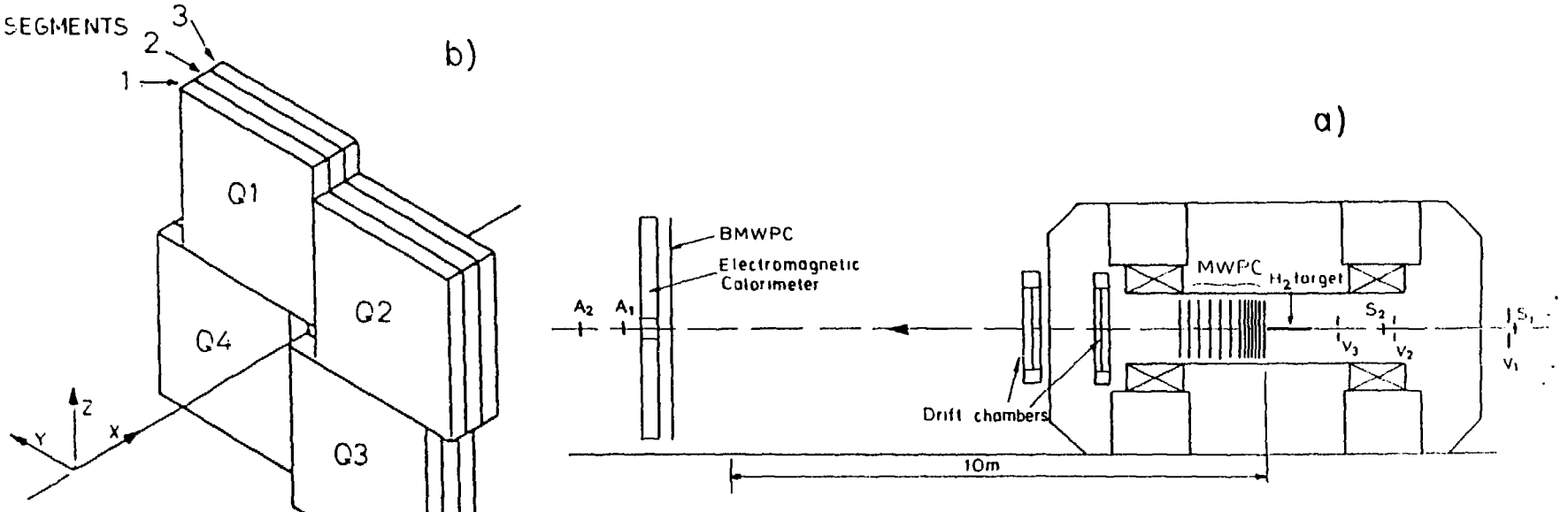
SEGMENTS
3
2
1
b)
Q1
Q2
Q3
Q4
Z
Y
X
a)
BMWPC
Electromagnetic
Calorimeter
A2
A1
MWPC
H2 target
S2
V3
V2
V1
Drift chambers
10m

FIG. 2

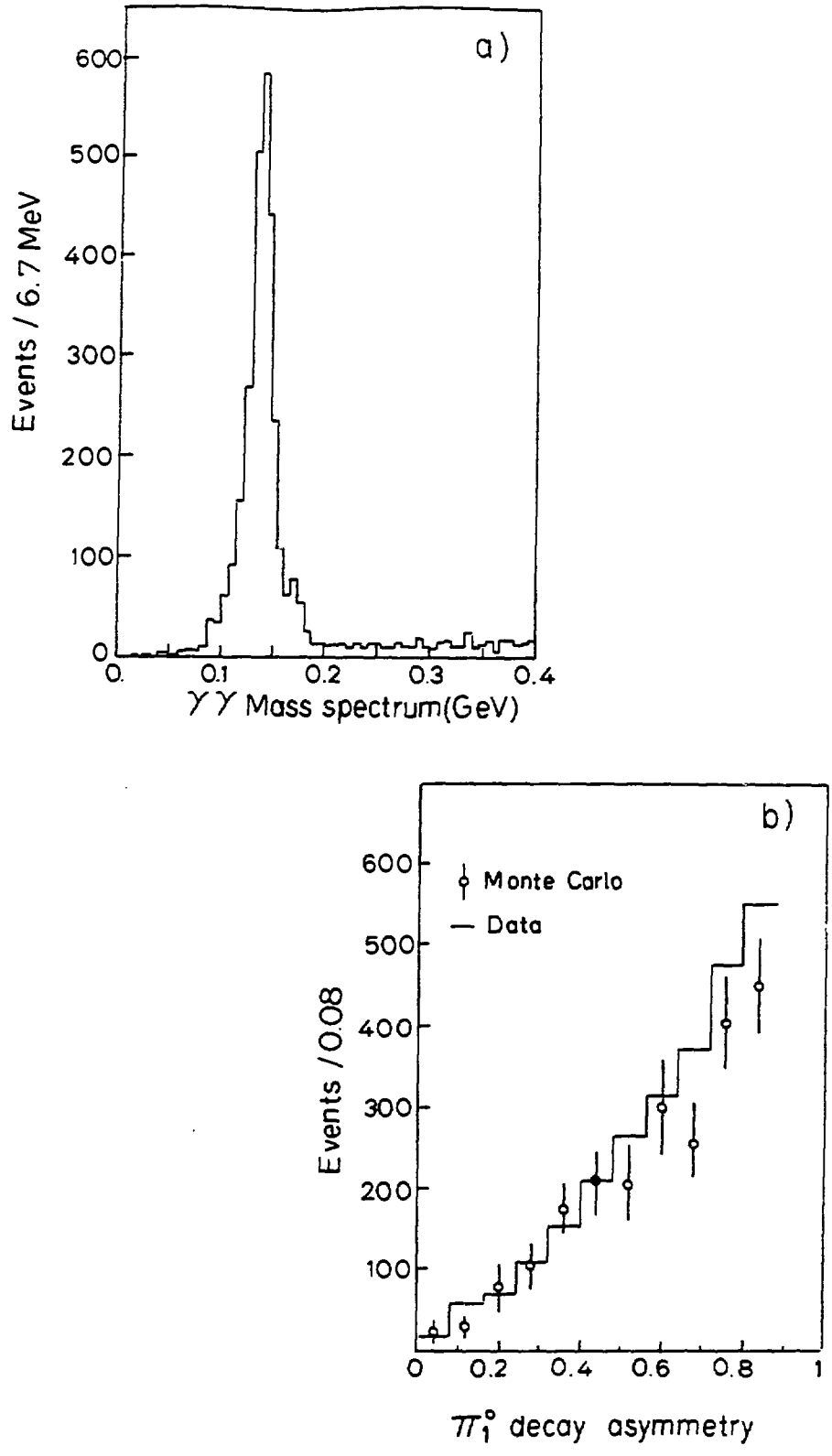
a)
Events / 6.7 MeV
600
500
400
300
200
100
0
0.
0.1
0.2
0.3
0.4
γγ Mass spectrum(GeV)
b)
Monte Carlo
Data
Events /0.08
600
500
400
300
200
100
0
0.2
0.4
0.6
0.8
1
π₁° decay asymmetry

FIG. 3

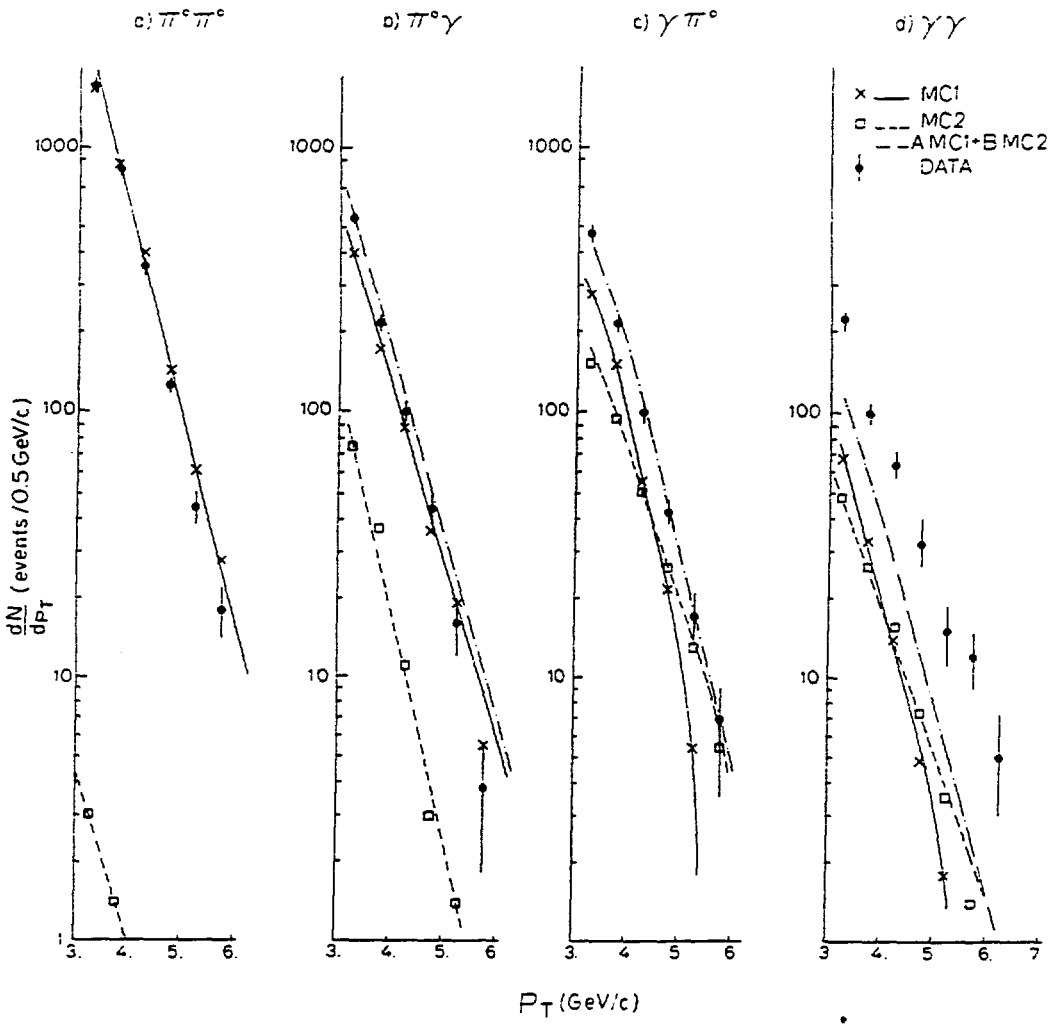
a) $\pi^0\pi^0$
b) $\pi^0\gamma$
c) $\gamma\pi^0$
d) $\gamma\gamma$
MC1
MC2
A MC1+B MC2
DATA
$\frac{dN}{dP_T}$ (events/0.5 GeV/c)
P_T (GeV/c)

FIG. 4

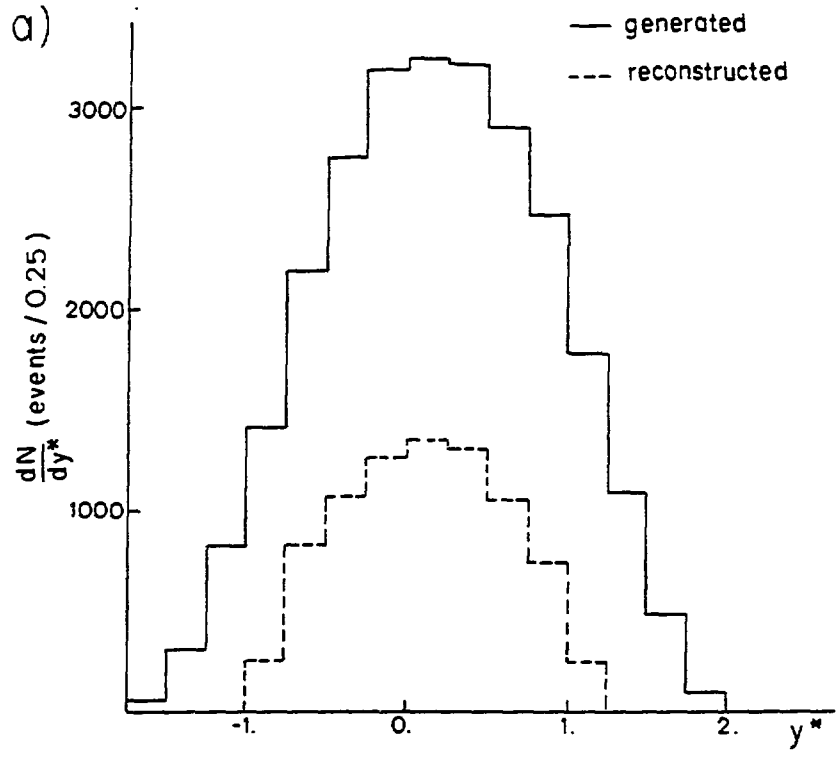
a)
generated
reconstructed
3000
2000
1000
dN/dy* (events / 0.25)
-1.
0.
1.
2.
y*

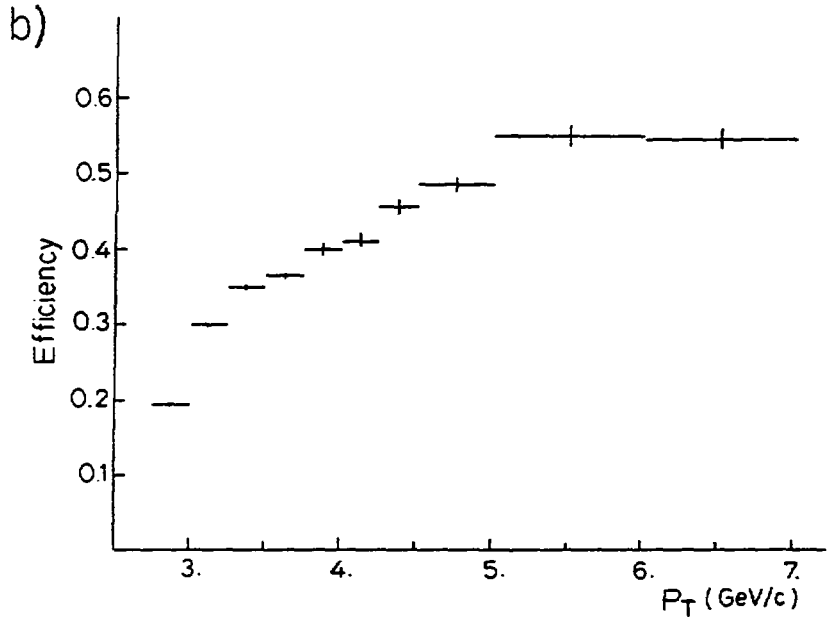
b)
0.6
0.5
0.4
0.3
0.2
0.1
Efficiency
3.
4.
5.
6.
7.
P_T (GeV/c)

FIG.5

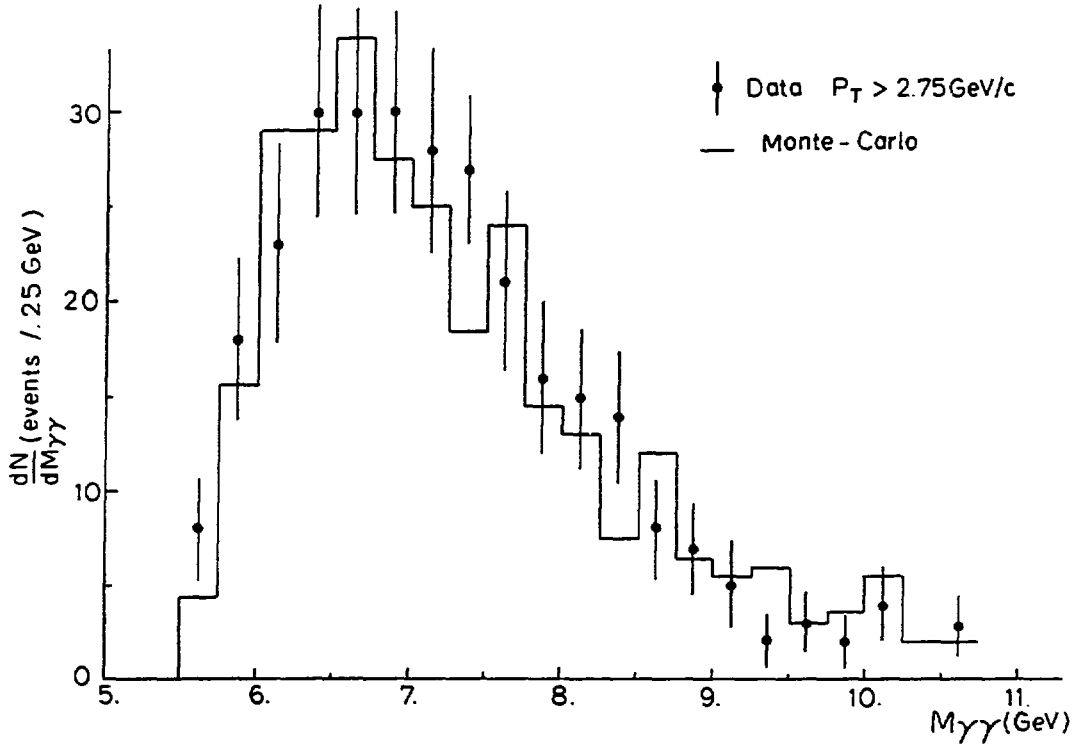
Data $P_T > 2.75$GeV/c
Monte - Carlo
$\frac{dN}{dM_{\gamma\gamma}}$ (events / .25 GeV)
30
20
10
0
5.
6.
7.
8.
9.
10.
11.
$M_{\gamma\gamma}$(GeV)

FIG. 6

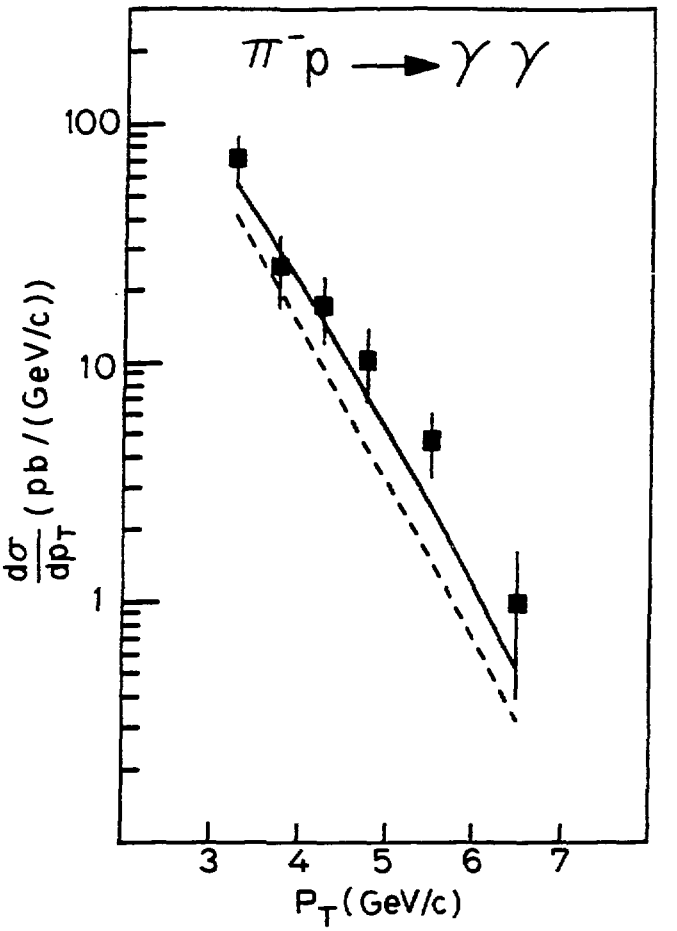

FIG. 7